Inhibition of TFG function causes hereditary axon degeneration by impairing endoplasmic reticulum structure

Christian Beetz[a], Adam Johnson[b], Amber L. Schuh[b], Seema Thakur[c], Rita-Eva Varga[a], Thomas Fothergill[d], Nicole Hertel[e], Ewa Bomba-Warczak[d], Holger Thiele[f], Gudrun Nürnberg[f], Janine Altmüller[f,g], Renu Saxena[h], Edwin R. Chapman[d], Erik W. Dent[d], Peter Nürnberg[f,g,i], and Anjon Audhya[b,1]

[a]Department of Clinical Chemistry and Laboratory Medicine, Jena University Hospital, 07747 Jena, Germany; [b]Department of Biomolecular Chemistry, University of Wisconsin School of Medicine and Public Health, Madison, WI 53706; [c]Department of Genetics and Fetal Medicine, Fortis La Femme, New Delhi 110048, India; [d]Department of Neuroscience, University of Wisconsin Medical School, Madison, WI 53706; [e]Institute of Anatomy I, Jena University Hospital, 07740 Jena, Germany; [f]Cologne Centre for Genomics, University of Cologne, 50931 Cologne, Germany; [g]Cologne Excellence Cluster on Cellular Stress Responses in Aging-Associated Diseases, University of Cologne, 50931 Cologne, Germany; [h]Centre of Medical Genetics, Sir Ganga Ram Hospital, New Delhi 110048, India; and [i]Center for Molecular Medicine Cologne, University of Cologne, 50931 Cologne, Germany

Edited by Charles Barlowe, Dartmouth Medical School, and accepted by the Editorial Board February 15, 2013 (received for review October 2, 2012)

Hereditary spastic paraplegias are a clinically and genetically heterogeneous group of gait disorders. Their pathological hallmark is a length-dependent distal axonopathy of nerve fibers in the corticospinal tract. Involvement of other neurons can cause additional neurological symptoms, which define a diverse set of complex hereditary spastic paraplegias. We present two siblings who have the unusual combination of early-onset spastic paraplegia, optic atrophy, and neuropathy. Genome-wide SNP-typing, linkage analysis, and exome sequencing revealed a homozygous c.316C>T (p.R106C) variant in the Trk-fused gene (*TFG*) as the only plausible mutation. Biochemical characterization of the mutant protein demonstrated a defect in its ability to self-assemble into an oligomeric complex, which is critical for normal TFG function. In cell lines, TFG inhibition slows protein secretion from the endoplasmic reticulum (ER) and alters ER morphology, disrupting organization of peripheral ER tubules and causing collapse of the ER network onto the underlying microtubule cytoskeleton. The present study provides a unique link between altered ER architecture and neurodegeneration.

membrane trafficking | COPII-mediated secretion | ER exit site

Hereditary spastic paraplegias (HSPs) are a diverse group of disorders characterized by spastic weakness in the lower extremities, which results from degeneration of upper motoneuron axons in the corticospinal tract (1, 2). Based on the presence or absence of other neurological abnormalities, HSPs are classified as complicated or pure, respectively. In addition to lower-limb spasticity, complicated forms of HSP may be associated with ataxia, mental retardation, dementia, extrapyramidal signs, visual dysfunction, and/or epilepsy. HSPs are typically progressive, but age of onset is highly variable. The heterogeneity in clinical presentation is accompanied by genetic heterogeneity. To date, more than 40 different genetic loci, which include nearly all modes of inheritance, have been linked to HSPs (1–5). However, in nearly half of these cases, the identities of the causative genes remain unknown. The identification of additional HSP genes and, more importantly, the functional characterization of their encoded products, will both contribute to our understanding of the pathomechanisms underlying HSPs and reveal the general requirements for lifelong axonal maintenance.

More than half the HSP cases in North America and Northern Europe can be attributed to defects in organelle dynamics (6). In particular, mutations that impact the architecture of the endoplasmic reticulum (ER) are common in patients with HSP. The ER is comprised of a network of membrane tubules and sheet-like cisternae that extend throughout the cytoplasm and encase the nucleus (7–9). Several factors contribute to this architecture, including (*i*) membrane-bending proteins of the REEP and reticulon families; (*ii*) regulators of the microtubule cytoskeleton, which governs the spatial patterning of the ER network; and (*iii*) components of the early secretory pathway that control vesicle biogenesis and egress (10–16). Among the best-characterized HSP genes are *SPAST*, *ATL1*, and *REEP1*, all of which encode proteins (spastin, atlastin-1, and REEP1, respectively) that potentially regulate ER organization. Mutations in *SPAST* were the first to be identified as a cause for autosomal dominant, uncomplicated HSP (17). Multiple studies indicate that spastin functions as a microtubule severing protein and can thereby regulate ER morphology (11, 18). Mutations in *ATL1*, which encodes a dynamin-related GTPase, are the second most common cause of uncomplicated HSP (19). Depletion of atlastin-1 perturbs ER structure and has been shown to inhibit axon elongation in rat cortical neurons (20, 21). *REEP1* mutations also cause an uncomplicated form of HSP (22). Together with reticulons, which have also been implicated in HSP (23), members of the REEP family are thought to generate and/or maintain the highly curved shape of ER membranes (7). Interestingly, spastin has been shown to interact biochemically with members of the atlastin, REEP, and reticulon families (11, 18, 24), suggesting that these proteins function together. Moreover, the consequences of mutations in the HSP-associated genes highlighted here suggest that proper ER organization likely plays a crucial role in axonal maintenance. However, it currently remains unclear which functions of the ER are necessary to prevent axon degeneration as observed in HSPs.

Results

We report on a family in which two of three siblings exhibit a combination of several neurological symptoms that is consistent with complicated HSP (Fig. 1*A*). Deliveries were uneventful and early developmental milestones were achieved on time. Pronounced leg spasticity, however, precluded the ability to walk independently. Vision problems were noted at 2.5 y of age and result from optic atrophy. Wasting of hand and leg muscles indicated additional neuropathy. In particular, clinical electrophysiology confirmed an axonal demyelinating motor neuropathy and revealed evidence for mild sensory involvement (Table S1). MRI performed on the older patient revealed no significant abnormalities (Table S2). At current ages of 16 and 12 y, both patients

Author contributions: C.B. and A.A. designed research; C.B., A.J., A.L.S., S.T., R.-E.V., T.F., N.H., E.B.-W., J.A., and A.A. performed research; C.B., R.S., E.R.C., E.W.D., P.N., and A.A. contributed new reagents/analytic tools; C.B., A.J., A.L.S., H.T., G.N., and A.A. analyzed data; and C.B. and A.A. wrote the paper.

The authors declare no conflict of interest.

This article is a PNAS Direct Submission. C.B. is a guest editor invited by the Editorial Board.

[1]To whom correspondence should be addressed. E-mail: audhya@wisc.edu.

This article contains supporting information online at www.pnas.org/lookup/suppl/doi:10.1073/pnas.1217197110/-/DCSupplemental.

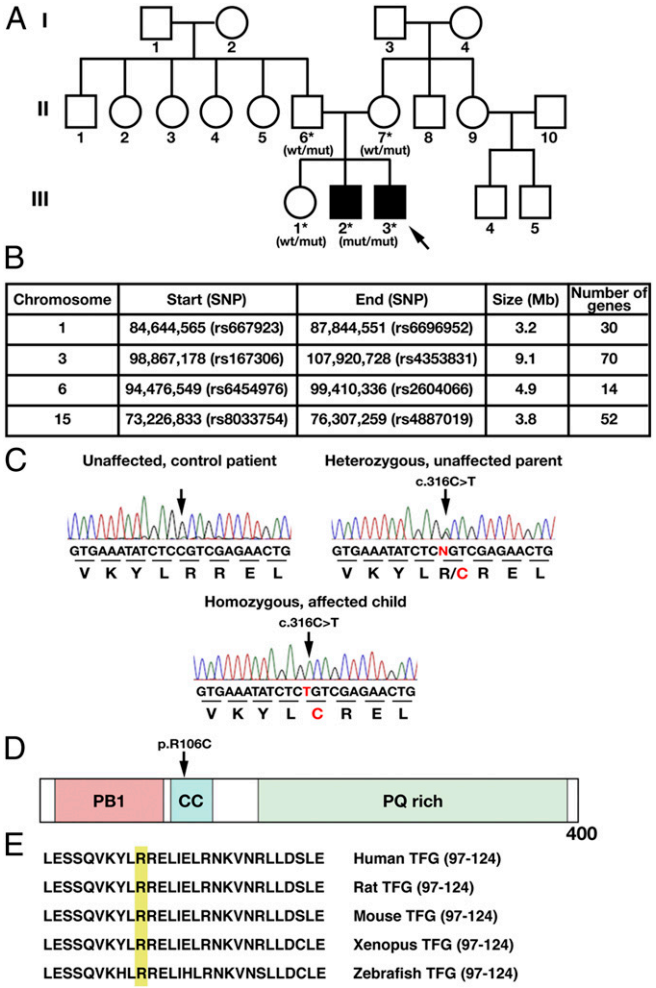

Chromosome	Start (SNP)	End (SNP)	Size (Mb)	Number of genes
1	84,644,565 (rs667923)	87,844,551 (rs6696952)	3.2	30
3	98,867,178 (rs167306)	107,920,728 (rs4353831)	9.1	70
6	94,476,549 (rs6454976)	99,410,336 (rs2604066)	4.9	14
15	73,226,833 (rs8033754)	76,307,259 (rs4887019)	3.8	52

Fig. 1. Association of a complicated form of hereditary spastic paraplegia with a homozygous missense alteration affecting a conserved residue of TFG. (*A*) Pedigree chart of a family affected by HSP. Filled and unfilled symbols indicate affected and unaffected individuals, respectively. Asterisks mark family members for whom DNA was available and who were applied in linkage analysis. Indicated below the identifiers are the results of *TFG* Sanger sequencing (mut, mutant allele; wt, WT allele). Arrow denotes the index case. (*B*) Runs of homozygosity >3 Mb and specific to the patients. (*C*) Exemplary results of Sanger sequencing of *TFG* exon 4 in an unaffected control patient, one of the affected parents, and the index case. (*D*) Schematic illustrating the domain organization of TFG. The alteration (p.R106C) detected in this study is highlighted. CC, coiled-coil domain; PB1, Phox and Bem1p domain; PQ rich, proline and glutamine-rich domain. (*E*) Amino acid sequence alignment of the TFG coiled-coil domain, showing the high level of conservation among different species.

are wheelchair-bound while the disease appears static. Further clinical details are summarized in Tables S3–S6.

The very unusual combination of symptoms including the corresponding ages of onset is highly reminiscent of spastic paraplegia, optic atrophy, neuropathy (SPOAN), a recessive form of HSP, which has so far only been described in a large, inbred Brazilian family (25). We therefore performed genome-wide SNP genotyping and analyzed in detail the SPOAN critical region on chromosome 11q13. No stretches of shared homozygosity overlapped with the SPOAN locus in our patients. A small region of ∼100 kb (chromosome 11: 59, 764, 149–159, 863, 602; build hg18) would be consistent with compound heterozygosity, but sequencing of the two corresponding genes (*MS4A4A*, *MS4AE6*) did not identify mutations.

Further analysis of the genotyping data indicated that all three siblings harbor numerous long runs of homozygosity (Table S7). Although the parents did not report consanguinity, run of homozygosity size and number strongly indicates recent parental relatedness (26). Consistent with this possibility, ancestors of both parents originate from a small geographic region in Northern India and belong to the same caste. We therefore introduced a consanguineous loop into the family, an approach successfully used in previous positional cloning projects in which consanguinity was only inferred (27), and performed genome-wide linkage analysis assuming recessive inheritance of a homozygous mutation. This revealed four regions with the maximum possible logarithm of odds score of 2.53 (Fig. 1*B*). Based on frequent association of mitochondrial dysfunction with optic atrophy (28, 29), we picked *TOMM70A* (chromosome 3 region; encoding a mitochondrial import translocator) (30) and *C6ORF66* (chromosome 6 region; previously implicated in mitochondrial complex I deficiency) (31) as candidates, but sequencing failed to identify potentially pathogenic variants.

To define the causative mutation, we performed whole-exome sequencing. A single homozygous variant was found in the regions of linkage as defined earlier. It affects the Trk-fused gene (*TFG*; c.316C>T) and was shown by Sanger sequencing to be homozygous in both patients, but heterozygous in the parents and the unaffected sibling (Fig. 1*C*). TFG was recently identified as a conserved regulator of protein secretion that assembles into an oligomeric matrix at the interface between the ER and ER–Golgi intermediate compartments in metazoans cells. It facilitates assembly of the COPII coat complex, required for membrane deformation and vesicle biogenesis from the ER, at least in part via its ability to form octamers in vivo (32). Interestingly, the variant identified alters a highly conserved residue within the TFG coiled-coil domain (p.R106C; Fig. 1 *D* and *E*), which plays an important role in TFG oligomerization (33). Analysis of mRNA samples from the family members indicated that the variant did not affect expression, suggesting that the mutant protein is likely to be synthesized similarly to the WT form. The variant was found neither by searching public variation databases (dbSNP-short genetic variations; National Heart, Lung, and Blood Institute Exome Variant Server; 1000 Genomes database) nor by sequencing of 100 local control individuals. We therefore conclude that the homozygous presence of c.316C>T in *TFG* underlies the symptoms observed in our patients. Accordingly, we have reserved the alias *SPG57* for spastic paraplegia caused by mutations in *TFG*.

In silico analysis predicts that the p.R106C mutation would disrupt the coiled-coil domain (PSORTII prediction). To determine the effect of the amino acid change directly, we expressed and purified a recombinant form of the full-length mutant protein for hydrodynamic studies. First, by using size-exclusion chromatography, we found the Stokes radii of WT and mutant (p.R106C) forms of TFG to be similar (Fig. S1 *A* and *B*). However, density gradient centrifugation studies indicated that the point mutation reduced the sedimentation value of the TFG oligomer (Fig. S1*C*). These data indicate that the p.R106C mutation perturbs the architecture of TFG complexes, but does not completely inhibit TFG self-association in vitro.

To further define the impact of the p.R106C mutation, we examined its influence on the oligomerization of the TFG amino terminus (amino acids 1–138) specifically. Based on its hydrodynamic and light scattering properties, we demonstrated that this region of TFG normally forms an octamer in solution (Fig. S1*D*), consistent with our previous results (32). We incorporated the single nucleotide change that causes HSP into a recombinant expression construct encoding the TFG amino terminus and isolated the mutant form of the protein in vitro. Compared with the WT TFG amino terminus, the mutant exhibited a reduced Stokes radius and sedimentation value (Fig. 2 *A* and *B*). Additionally, we used multiangle light scattering to further confirm the change in TFG complex formation. These studies highlighted that a significant fraction of the TFG mutant fails to assemble into an octamer (Fig. 2*C*). This finding was further confirmed by studying the effect

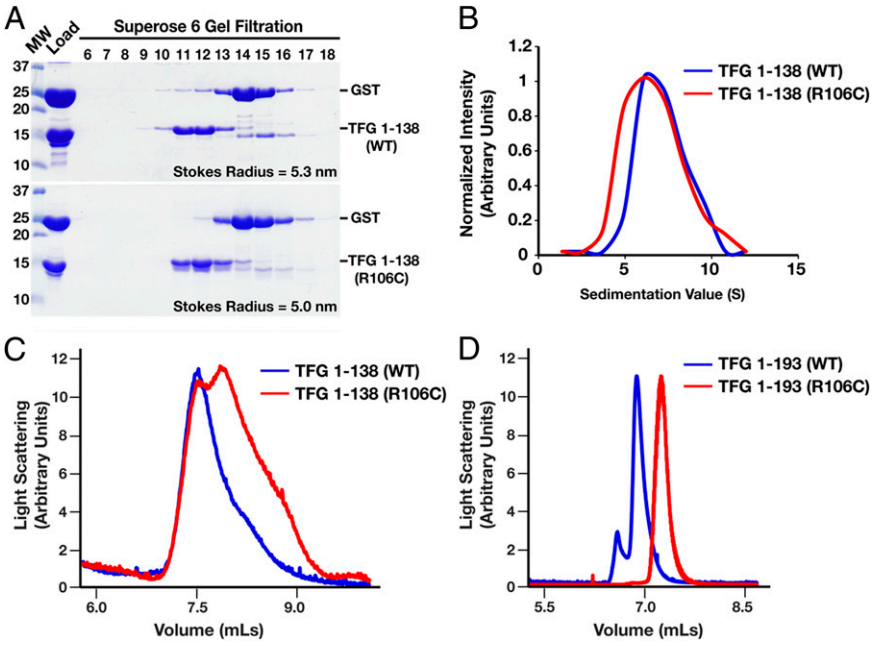

Fig. 2. Mutant p.R106C isoforms of TFG exhibit defects in normal oligomerization in vitro. (*A*) Purified GST-fused forms of WT and p.R106C TFG (amino acids 1–138) were cleaved in solution to remove the tag and separated by size-exclusion chromatography. Eluted fractions were separated by SDS/PAGE and stained with Coomassie stain. The Stokes radius of each protein was determined based on the elution profile of characterized standards. (*B*) Purified proteins described in *A* were applied to a glycerol density gradient (10–30%) and fractionated by hand. Individual fractions recovered were separated by SDS/PAGE and stained by using Coomassie stain. Densitometry measurements were made to quantify the amount of protein in each fraction, which is presented in a graphical format. (*C* and *D*) WT and p.R106C TFG (amino acids 1–138 and 1–193) were purified and examined by light scattering following size-exclusion chromatography. The lack of overlap between the peaks for each pair indicates that the oligomerization of TFG is altered in the presence of the R106C mutation.

of the p.R106C mutation on the self-association of a larger TFG fragment encoding amino acids 1 to 193 (Fig. 2*D*). Together, these studies demonstrate that the p.R106C mutation perturbs normal assembly of TFG complexes, which is critical for TFG function (32, 33), and highlights a mechanistic basis for the mutation that results in HSP.

To define sites of TFG expression, we conducted in situ hybridization experiments on sectioned mouse embryos. Consistent with the neurodegenerative phenotype in our patients, we observed high levels of *TFG* expression in the central nervous system and the eye (Fig. 3*A*). These findings corroborate recent data acquired by using immunohistochemistry and RT-PCR (34).

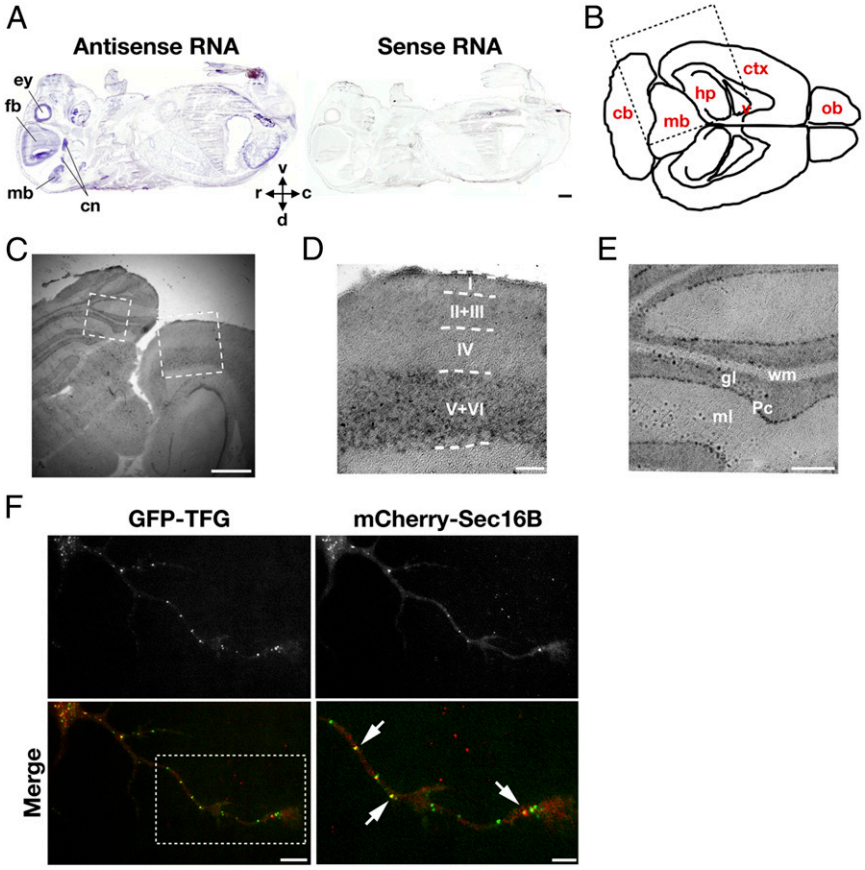

Fig. 3. TFG is highly expressed in the brain cortex and accumulates at ER exit sites in cultured murine neurons and human epithelial cells. (*A*) Sagittal section of a murine embryo (embryonic day 16) hybridized in situ with *TFG*-specific antisense (*Left*) and sense (*Right*) RNA probes. c, caudal; cn, cranial nerve ganglia; d, dorsal; ey, eye; fb, forebrain; mb, midbrain; r, rostral; v, ventral. (Scale bar, 1 mm.) (*B*) Cartoon illustrating a horizontal brain section from an adult mouse at Bregma – 3.4 mm. cb, cerebellum; ctx, cortex; hp, hippocampus; mb, midbrain; ob, olfactory bulb; v, ventricle. (*C*) *TFG*-specific in situ hybridization of an area corresponding to the region boxed in *B*. (Scale bar, 1 mm.) (*D*) Magnification of the cortical area marked by the right box in *C*. Roman numerals indicate cortical layers. (Scale bar, 200 μm.) (*E*) Magnification of the cerebellar area marked by left box in *C*. gl, granular layer; ml, molecular layer; Pc, Purkinje cell layer; wm, white matter. (Scale bar, 200 μm.) (*F*) Murine neurons transfected with plasmids encoding GFP-TFG and mCherry-Sec16B were imaged by using total internal reflection fluorescence microscopy. (Scale bar, 10 μm.) (*Lower Right*) A 1.8× zoom of the boxed region. Arrows highlight ER exit sites at which TFG and Sec16B colocalize. (Scale bar, 5 μm.)

In particular, our analysis of the adult murine brain (Fig. 3 *B–E*) and the previous protein-based study (34) indicate that TFG is highly abundant in Purkinje cells, which are essential for motor function. Moreover, we observed similarly strong expression of TFG in deep cortical layers, including layer V, the region harboring the somata of motoneurons in the motor cortex (Fig. 3*D*). This pattern of expression correlates well with the movement disorders exhibited by our patients.

We further conducted high-resolution total internal reflection fluorescence (TIRF) imaging of subcellular TFG distribution in cultured murine cortical neurons. These studies highlighted the presence of TFG in punctate structures, several of which colocalized with Sec16, a marker of ER exit sites (35, 36), both in axons and dendrites (Fig. 3*F* and Fig. S2*A*). Live cell imaging of neuritic growth cones showed TFG to be highly dynamic, typically associating with ER tubules that underwent numerous extensions and retractions over time (Movie S1). To determine whether the p.R106C mutation affects the localization of TFG, we expressed the mutant protein as a GFP fusion in cultured epithelial cells (GFP-TFG^{R106C}). Similar to WT, mutant TFG accumulated at ER exit sites, colocalizing with Sec16 (Fig. S2 *B* and *C*). Consistent with these data, the localization and dynamics of GFP-TFG^{R106C} in murine neurons was indistinguishable from that of WT GFP-TFG (Movie S2). Importantly, specific depletion of endogenous TFG by using siRNAs targeting its unique 3′UTR did not perturb the localization of GFP-TFG^{R106C} in epithelia cells (Fig. S2*D*). These studies collectively indicate that the p.R106C mutation does not affect TFG localization significantly. Instead, it impairs normal TFG structure and thereby affects its function at ER exit sites.

Our previous work showed that TFG depletion inhibits secretory cargo egress from the ER in human cells and also leads to ER fragmentation in *Caenorhabditis elegans* oocytes (32). To further determine the effect of TFG inhibition on the ER in cultured mammalian cells, we used validated siRNAs to reduce TFG levels by ∼80% in COS7 cells, an ideal model for the study of ER dynamics (Fig. 4*A*). Consistent with our previous studies in *C. elegans* (32), we found that the highly branched organization of the tubular ER network was altered following TFG depletion, and the abundant three-way junctions characteristic of control cells were difficult to resolve subsequent to TFG siRNA treatment (Fig. S3). Moreover, we found that peripheral ER tubules collapsed onto the microtubule cytoskeleton in TFG-depleted cells, as indicated by their increased level of overlap relative to control cells (Fig. 4 *B* and *C*). Specifically, there was a significant elevation in the degree of colocalization between tubulin and calreticulin as measured by Pearson correlation coefficient (0.34 ± 0.09 in control cells and 0.83 ± 0.14 in depleted cells; $P < 0.01$; $n = 12$ cells per condition). The distribution of mitochondria, which is partially dependent upon ER organization (37), was also impacted. Unlike control cells, which contain mitochondria scattered throughout the cytoplasm, TFG-depleted cells exhibited clustering of mitochondria around the microtubule organizing center, with few extending into the cell periphery (Fig. 4*D*). In contrast to these defects in organelle morphology and distribution, there was little or no effect on organization or bundling of microtubules in TFG-depleted cells, indicating that the changes observed were not an indirect consequence of perturbing the microtubule cytoskeleton (Fig. 4 *E* and *F*). Collectively, our data indicate that interfering with normal TFG function disrupts ER organization, which potentially results from impaired vesicle transport in the early secretory pathway.

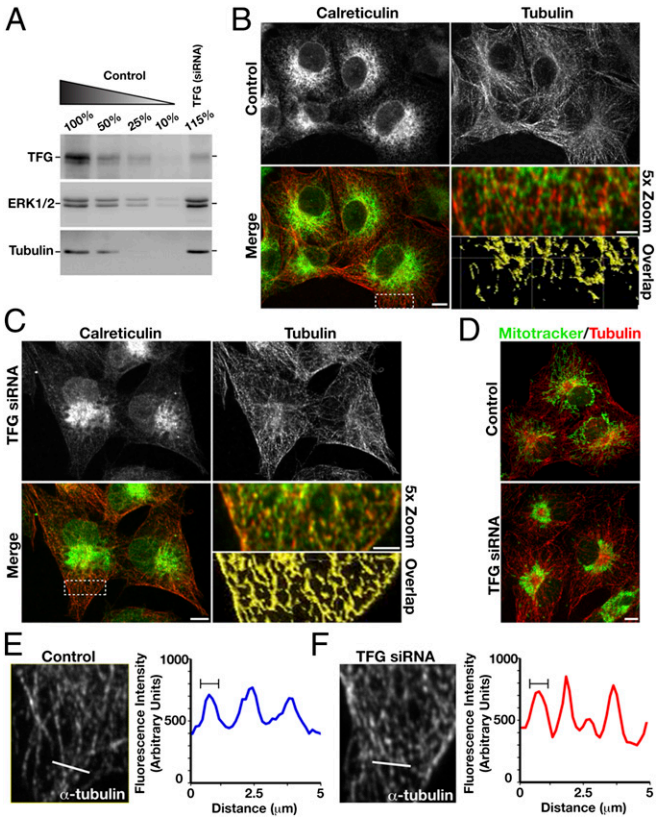

Fig. 4. Depletion of TFG disrupts ER architecture and distribution of mitochondria in mammalian cells. (*A*) Immunoblots of extracts prepared from COS7 cells depleted of TFG by siRNA. Serial dilutions of extracts prepared from control cells were loaded to quantify depletion levels. Blotting with antibodies directed against ERK1/2 and tubulin were performed to control loading. (*B–D*) COS7 cells that were transfected with siRNAs targeting TFG or mock-transfected were fixed and stained by using antibodies directed against calreticulin and tubulin and imaged by using swept-field confocal optics. Cells were incubated with MitoTracker before fixation to stain mitochondria (*D*). (Scale bars, 5 μm.) Additionally, a 5× zoom of a boxed region of the peripheral ER (*B* and *C*) is provided. Color overlays show the ER (green) relative to microtubules (red). (Scale bars, 2 μm.) By using Imaris software, we specifically identified the areas of overlap in the boxed regions, which highlight differences in ER–microtubule associations in control cells compared with cells treated with TFG siRNA (*B* and *C*, *Bottom Right*). (*E* and *F*) Cropped images of microtubules in control (*E*) and TFG-depleted (*F*) cells. Line scan analysis (examined region highlighted with a 5-μm white line) was used to demonstrate that the thickness of peripheral microtubules, as determined by their fluorescence intensity, does not vary between the conditions. Data shown are representative of the population ($n = 23$ cells analyzed per condition).

Discussion

TFG was first identified as a fusion partner of the neurotrophic tyrosine kinase receptor type 1 (*NTRK1*) in human papillary carcinoma, which resulted from a translocation event between chromosomes 1 and 3 (38). Subsequently, additional TFG fusion proteins were isolated from other malignancies, all of which involved the oligomeric amino terminus of TFG (39, 40). We recently demonstrated that native TFG functions at sites of vesicle biogenesis on the ER, forming a matrix between ER exit sites and the ER–Golgi intermediate compartment, a key sorting hub for secretory cargoes in metazoan cells (32). In the present study, we identify an additional important physiological function for TFG in long-term axonal maintenance.

Our work demonstrates that a mutation in TFG (p.R106C) causes a recessive form of complicated HSP. Interestingly, TFG was also recently implicated in autosomal-dominant hereditary motor and sensory neuropathy with proximal dominant involvement (41). In contrast to the TFG mutation we characterized, the contemporary study identified an amino acid change (p.P285L) in the carboxyl-terminal P/Q-rich domain. Pathological studies showed the presence of cytoplasmic neuronal inclusions, which were positive not only for TFG, but also for ubiquitin and sometimes TAR DNA-binding protein 43 kDa (TDP-43), a protein associated with several motor neuron diseases including

amyotrophic lateral sclerosis and frontotemporal dementia (42,43). These inclusions may mediate a toxic gain-of-function effect, resulting in a dominant inheritance pattern. In combination with our findings, these data conclusively implicate TFG dysfunction in neurodegeneration, emphasizing roles for TFG in upper motor neurons (as shown in the present study), as well as lower motor neurons and sensory neurons (41). Notably, this set of neurons, which possess extremely long axons, is also affected by mutations in several other genes that have been previously implicated in neurodegenerative disorders. Two recurrent missense mutations in Berardinelli-Seip congenital lipodystrophy 2 (*BSCL2*) are associated with a clinical spectrum ranging from pure HSP to pure distal motor neuropathy (44). Similarly, mutations in *ATL1* have been linked to pure HSP, but can also result in motor neuropathy with sensory involvement (45–47). In the case of *REEP1*, distinct mutations have been shown to give rise to defects that affect only upper motoneurons (22) or only lower motoneurons (48), similar to the disparate effects of the two unique mutations identified in *TFG*. Strikingly, all these factors function at the ER. Moreover, the aberrant redistribution of the ER along microtubules observed following TFG depletion is also seen upon overexpression of REEP1 or an HSP-causing form of spastin that lacks ATPase activity (p.K388R) (11,18). Depletion of atlastin-1 was shown to promote the formation of long, unbranched ER tubules (45), which may also be juxtaposed tightly to microtubules, even though this has not been directly examined. Nevertheless, the lack of ER branching is again similar to the phenotype we observed in TFG-depleted cells. Together, our collective data suggest that changes in ER architecture, which alter its dynamic association with microtubules, are tightly coupled to the pathology of HSPs, strongly supporting the emerging concept that ER structure and function play critical roles in neuronal maintenance (8).

Unlike other genes that have been linked to HSP, *TFG* encodes a protein that functions directly in the regulation of COPII vesicle secretion (32). As ER organization and vesicle secretion are tightly coupled, it is difficult to dissect their relative contributions to neuron health. The phenotypes exhibited by patients with the p.R106C mutation in TFG are more severe than those associated with pure forms of the disease that can result from mutations in *SPAST*, *ATL1*, or *REEP1*. By comparison, the patients we studied were substantially more similar to those with a complicated form of HSP known as SPOAN (25). Analysis of the genes within this region revealed the presence of at least three that are known to function in ER morphogenesis: RAB1B (a Rab-type GTPase required for vesicle secretion from the ER), YIF1A (a transmembrane protein also implicated in the early secretory pathway), and RTN3 (a member of the reticulon family of ER shaping proteins) (49–51). Sequence analysis of these genes in patients with SPOAN will be enlightening, and may help to confirm a specific requirement for secretory transport from the ER in maintenance of neuronal integrity.

Materials and Methods

Patients and Controls. Approval for this study was obtained from the ethics review board at the Fortis La Femme Hospital. The family studied sought genetic counseling and was referred to Fortis La Femme Hospital in New Delhi, India. After informed consent was obtained, DNA was extracted from peripheral blood samples. Total RNA was prepared by applying the PAXgene blood RNA kit (Qiagen). One hundred anonymized DNA samples from another New Delhi Hospital served as local controls.

Haplotyping, Linkage Analysis, and DNA Sequencing. DNA samples from the two affected patients, their parents, and their unaffected sister were genotyped by using the Genome-Wide Human SNP Array 6.0 (Affymetrix). Genders were verified by counting heterozygous SNPs on the X chromosome. Relationship errors were evaluated with the help of the program Graphical Relationship Representation (52). The program PedCheck was applied to detect Mendelian errors (53), and data for SNPs with such errors were removed from the data set. Non-Mendelian errors were identified by using the program MERLIN (54), and unlikely genotypes for related samples were deleted. Linkage analysis was performed by introducing a second-degree cousin loop for the patients' parents and assuming autosomal-recessive inheritance, full penetrance, and a disease gene frequency of 0.0001. Multipoint logarithm of odds scores were calculated and haplotypes reconstructed in the program ALLEGRO (55). All data handling was performed by using the graphical user interface ALOHOMORA (56). For exome sequencing, genomic DNA was fragmented by sonication, end-repaired, and adaptor-ligated. The first version of the NimbleGen Sequence Capture Human Exome 2.1M Array (Roche NimbleGen) was used for enrichment of exonic and adjacent intronic sequences comprising in total 34 Mb of target sequence. Enriched DNA was then sequenced by using an Illumina HiSEq 2000 instrument. Mean coverage was 299-fold, and 98% of the target sequence was covered at least 30-fold. Variants initially detected were filtered against public variation databases and a set of in-house exomes. Subsequently, only variants residing in the regions of linkage (covered at least fourfold) and showing a minimum frequency of 75% were kept. Primers applied in Sanger sequencing are available upon request.

In Situ Hybridization. A 536-bp RT-PCR product corresponding to nucleotides 685–1220 of murine TFG (NM_019678.2) was cloned into pCR II-TOPO. After linearization, sense and antisense cRNAs were transcribed by T7 and SP6 RNA polymerases, respectively. cRNAs were labeled with digoxigenin (DIG RNA Labeling Kit; Roche Diagnostics) according to the manufacturer's instructions. Sections (20 μm) from whole embryos (embryonic day 16) and adult brain (4 mo) were obtained from fresh frozen samples of C57BL/6 mice, thawed onto glass slides, and hybridized with the labeled cRNAs as described previously (57).

Preparation and Transfection of Primary Murine Neurons. All mouse procedures were approved by the University of Wisconsin Committee on Animal Care and were in accordance with National Institutes of Health guidelines. Cortical neuron cultures were prepared from embryonic day 15 Swiss Webster mice (Taconic) (58). Brains were removed and cortices dissected out, and meninges removed before being trypsinized and dissociated. Dissociated cortical neurons were plated directly onto poly-D-lysine–coated dishes, or transfected before plating with 5 μg each of GFP-TFG, mCherry-Sec16B, and ER-tdTomato plasmids. Transfection was performed by resuspending cells in Nucleofector solution (Mouse Neuron Kit; Lonza) along with plasmid DNA, and electroporated by using a Lonza Nucleofector according to the manufacturer's directions. Neurons were transferred into plating medium [Neurobasal medium with 5% (vol/vol) FBS, B27 supplement, 2 mM glutamine, 37.5 mM NaCl, and 0.3% glucose] and plated on 0.1 mg/mL poly-D-lysine–coated glass coverslips in six-well plates, or adhered to the bottom of 35-mm plastic culture dishes that had a 15-mm hole drilled through the bottom of the chamber for live TIRF imaging. After 1 h, this medium was replaced with serum-free medium (plating medium lacking FBS).

Immunofluorescence, Live Cell Imaging, and Depletion Studies. Confocal images were acquired on a swept-field confocal microscope (Ti-E; Nikon) equipped with a Roper CoolSnap HQ2 CCD camera using a Nikon 60×, 1.4 NA plan apo oil objective lens. TIRF imaging was conducted on a Nikon TE2000E equipped with a TIRF illuminator, a 100×, 1.49 NA plan apo TIRF objective, a Perfect Focus System, a temperature-controlled stage, and a CoolSnap HQ CCD camera. Acquisition parameters and image analysis (including line scan measurements) was performed by using Nikon Elements (confocal) or Metamorph (TIRF) software. For imaging fixed cortical neurons, cells were grown in vitro for 2 d before being fixed in 4% (vol/vol) paraformaldehyde/Krebs/sucrose at 37 °C for 20 min. Cultures were rinsed in PBS solution and blocked with 10% (vol/vol) BSA/PBS solution, permeabilized in 0.2% Triton X-100/PBS solution, and labeled with anti-TFG or anti-Sec16A antibodies and anti-tyrosinated tubulin and Alexa 488- or 546-conjugated secondary antibodies. For wide-field imaging, neurons were imaged on a Nikon TE2000 inverted microscope as described previously (59). Imaging of RPE1 and COS7 cells was conducted following fixation by using a similar procedure to that described for neuron cultures. Labeling was conducted using anti-calreticulin and anti-tubulin antibodies and Cy3- or Cy5-conjugated secondary antibodies. Fluorescently tagged proteins did not require signal amplification using antibody staining. For analysis of mitochondria distribution, MitoTracker (Invitrogen) was added to cells before fixation. TFG depletion studies were carried out by using siRNAs targeting human TFG that were transfected by using Lipofectamine RNAiMAX as described previously (33).

Biochemistry. Recombinant protein expression was performed by using BL21 (DE3) *Escherichia coli*, and purifications were conducted by using glutathione agarose beads for GST fusions proteins. Glycerol gradients (10–30%) were poured using a Gradient Master and fractionated from

the top by hand. A 4-mL gradient [10–30% (vol/vol) glycerol] was generated by using a Gradient Master, and 200-μL fractions were collected by hand from the top of the gradient. In all cases, one 20th of the fractions were separated by SDS/PAGE and stained with Coomassie stain. Sedimentation values were calculated by comparing the position of the peak with that of characterized standards run on a separate gradient in parallel. For size-exclusion chromatography, 1-mL samples were loaded onto a Superose 6 column or an S200 column, and 1-mL fractions were subsequently collected. In all cases, one 100th of the fractions were separated by SDS/PAGE and stained with Coomassie stain. The Stokes radius of each protein was calculated from its elution volume based on the elution profiles of characterized standards. Light-scattering data were collected by using a Wyatt miniDAWN TREOS three-angle light-scattering detector, which was coupled to a high-resolution size-exclusion chromatography column. Data were collected every second at a flow rate of 0.5 mL/min and analyzed by using ASTRA software to determine the molecular mass of macromolecules (60). Immunoblot analysis to quantify the level of TFG depletion was conducted as described previously (33).

ACKNOWLEDGMENTS. We thank Dr. Gia Voeltz for providing constructs to visualize the ER and members of the A.A. laboratory. for critical reading of this manuscript. This work was supported by National Institutes of Health Grants 1R01GM088151-01A1 (to A.A.) and R01NS064014 (to E.W.D.). E.R.C. is an investigator of the Howard Hughes Medical Institute.

1. Blackstone C, O'Kane CJ, Reid E (2011) Hereditary spastic paraplegias: Membrane traffic and the motor pathway. *Nat Rev Neurosci* 12(1):31–42.
2. Schüle R, Schöls L (2011) Genetics of hereditary spastic paraplegias. *Semin Neurol* 31(5):484–493.
3. Fink JK (2006) Hereditary spastic paraplegia. *Curr Neurol Neurosci Rep* 6(1):65–76.
4. Salinas S, Proukakis C, Crosby A, Warner TT (2008) Hereditary spastic paraplegia: clinical features and pathogenetic mechanisms. *Lancet Neurol* 7(12):1127–1138.
5. Ikenaka K, et al. (2012) Disruption of axonal transport in motor neuron diseases. *Int J Mol Sci* 13(1):1225–1238.
6. Soderblom C, Blackstone C (2006) Traffic accidents: Molecular genetic insights into the pathogenesis of the hereditary spastic paraplegias. *Pharmacol Ther* 109(1-2):42–56.
7. Friedman JR, Voeltz GK (2011) The ER in 3D: A multifunctional dynamic membrane network. *Trends Cell Biol* 21(12):709–717.
8. Renvoisé B, Blackstone C (2010) Emerging themes of ER organization in the development and maintenance of axons. *Curr Opin Neurobiol* 20(5):531–537.
9. Voeltz GK, Rolls MM, Rapoport TA (2002) Structural organization of the endoplasmic reticulum. *EMBO Rep* 3(10):944–950.
10. Voeltz GK, Prinz WA, Shibata Y, Rist JM, Rapoport TA (2006) A class of membrane proteins shaping the tubular endoplasmic reticulum. *Cell* 124(3):573–586.
11. Park SH, Zhu PP, Parker RL, Blackstone C (2010) Hereditary spastic paraplegia proteins REEP1, spastin, and atlastin-1 coordinate microtubule interactions with the tubular ER network. *J Clin Invest* 120(4):1097–1110.
12. Audhya A, Desai A, Oegema K (2007) A role for Rab5 in structuring the endoplasmic reticulum. *J Cell Biol* 178(1):43–56.
13. Valenzuela JI, Jaureguiberry-Bravo M, Couve A (2011) Neuronal protein trafficking: Emerging consequences of endoplasmic reticulum dynamics. *Mol Cell Neurosci* 48(4):269–277.
14. Park SH, Blackstone C (2010) Further assembly required: Construction and dynamics of the endoplasmic reticulum network. *EMBO Rep* 11(7):515–521.
15. Dykstra KM, Pokusa JE, Suhan J, Lee TH (2010) Yip1A structures the mammalian endoplasmic reticulum. *Mol Biol Cell* 21(9):1556–1568.
16. Zanetti G, Pahuja KB, Studer S, Shim S, Schekman R (2012) COPII and the regulation of protein sorting in mammals. *Nat Cell Biol* 14(1):20–28.
17. Hazan J, et al. (1999) Spastin, a new AAA protein, is altered in the most frequent form of autosomal dominant spastic paraplegia. *Nat Genet* 23(3):296–303.
18. Connell JW, Lindon C, Luzio JP, Reid E (2009) Spastin couples microtubule severing to membrane traffic in completion of cytokinesis and secretion. *Traffic* 10(1):42–56.
19. Zhao X, et al. (2001) Mutations in a newly identified GTPase gene cause autosomal dominant hereditary spastic paraplegia. *Nat Genet* 29(3):326–331.
20. Zhu PP, Soderblom C, Tao-Cheng JH, Stadler J, Blackstone C (2006) SPG3A protein atlastin-1 is enriched in growth cones and promotes axon elongation during neuronal development. *Hum Mol Genet* 15(8):1343–1353.
21. Bian X, et al. (2011) Structures of the atlastin GTPase provide insight into homotypic fusion of endoplasmic reticulum membranes. *Proc Natl Acad Sci USA* 108(10):3976–3981.
22. Züchner S, et al. (2006) Mutations in the novel mitochondrial protein REEP1 cause hereditary spastic paraplegia type 31. *Am J Hum Genet* 79(2):365–369.
23. Montenegro G, et al. (2012) Mutations in the ER-shaping protein reticulon 2 cause the axon-degenerative disorder hereditary spastic paraplegia type 12. *J Clin Invest* 122(2):538–544.
24. Mannan AU, et al. (2006) Spastin, the most commonly mutated protein in hereditary spastic paraplegia interacts with Reticulon 1 an endoplasmic reticulum protein. *Neurogenetics* 7(2):93–103.
25. Macedo-Souza LI, et al. (2005) Spastic paraplegia, optic atrophy, and neuropathy is linked to chromosome 11q13. *Ann Neurol* 57(5):730–737.
26. Pemberton TJ, et al. (2012) Genomic patterns of homozygosity in worldwide human populations. *Am J Hum Genet* 91(2):275–292.
27. Crisponi L, et al. (2007) Crisponi syndrome is caused by mutations in the CRLF1 gene and is allelic to cold-induced sweating syndrome type 1. *Am J Hum Genet* 80(5):971–981.
28. Newman NJ (2005) Hereditary optic neuropathies: from the mitochondria to the optic nerve. *Am J Ophthalmol* 140(3):517–523.
29. Kwong JQ, Beal MF, Manfredi G (2006) The role of mitochondria in inherited neurodegenerative diseases. *J Neurochem* 97(6):1659–1675.
30. Edmonson AM, Mayfield DK, Vervoort V, DuPont BR, Argyropoulos G (2002) Characterization of a human import component of the mitochondrial outer membrane, TOMM70A. *Cell Commun Adhes* 9(1):15–27.
31. Saada A, et al. (2008) C6ORF66 is an assembly factor of mitochondrial complex I. *Am J Hum Genet* 82(1):32–38.
32. Witte K, et al. (2011) TFG-1 function in protein secretion and oncogenesis. *Nat Cell Biol* 13(5):550–558.
33. Greco A, et al. (1998) Role of the TFG N-terminus and coiled-coil domain in the transforming activity of the thyroid TRK-T3 oncogene. *Oncogene* 16(6):809–816.
34. Maebayashi H, et al. (2012) Expression and localization of TRK-fused gene products in rat brain and retina. *Acta Histochem Cytochem* 45(1):15–23.
35. Connerly PL, et al. (2005) Sec16 is a determinant of transitional ER organization. *Curr Biol* 15(16):1439–1447.
36. Watson P, Townley AK, Koka P, Palmer KJ, Stephens DJ (2006) Sec16 defines endoplasmic reticulum exit sites and is required for secretory cargo export in mammalian cells. *Traffic* 7(12):1678–1687.
37. Palmer CS, Osellame LD, Stojanovski D, Ryan MT (2011) The regulation of mitochondrial morphology: Intricate mechanisms and dynamic machinery. *Cell Signal* 23(10):1534–1545.
38. Greco A, et al. (1995) The DNA rearrangement that generates the TRK-T3 oncogene involves a novel gene on chromosome 3 whose product has a potential coiled-coil domain. *Mol Cell Biol* 15(11):6118–6127.
39. Hernández L, et al. (1999) TRK-fused gene (TFG) is a new partner of ALK in anaplastic large cell lymphoma producing two structurally different TFG-ALK translocations. *Blood* 94(9):3265–3268.
40. Hisaoka M, Ishida T, Imamura T, Hashimoto H (2004) TFG is a novel fusion partner of NOR1 in extraskeletal myxoid chondrosarcoma. *Genes Chromosomes Cancer* 40(4):325–328.
41. Ishiura H, et al. (2012) The TRK-fused gene is mutated in hereditary motor and sensory neuropathy with proximal dominant involvement. *Am J Hum Genet* 91(2):320–329.
42. Rademakers R, Neumann M, Mackenzie IR (2012) Advances in understanding the molecular basis of frontotemporal dementia. *Nat Rev Neurol* 8(8):423–434.
43. Lagier-Tourenne C, Cleveland DW (2009) Rethinking ALS: The FUS about TDP-43. *Cell* 136(6):1001–1004.
44. Auer-Grumbach M, et al.; Austrian Peripheral Neuropathy Study Group (2005) Phenotypes of the N88S Berardinelli-Seip congenital lipodystrophy 2 mutation. *Ann Neurol* 57(3):415–424.
45. Hu J, et al. (2009) A class of dynamin-like GTPase involved in the generation of the tubular ER network. *Cell* 138:5489–5561.
46. Ivanova N, et al. (2007) Hereditary spastic paraplegia 3A associated with axonal neuropathy. *Arch Neurol* 64(5):706–713.
47. Guelly C, et al. (2011) Targeted high-throughput sequencing identifies mutations in atlastin-1 as a cause of hereditary sensory neuropathy type I. *Am J Hum Genet* 88(1):99–105.
48. Beetz C, et al. (2012) Exome sequencing identifies a REEP1 mutation involved in distal hereditary motor neuropathy type V. *Am J Hum Genet* 91(1):139–145.
49. Slavin I, et al. (2011) Role of Rab1b in COPII dynamics and function. *Eur J Cell Biol* 90(4):301–311.
50. Yoshida Y, et al. (2008) YIPF5 and YIF1A recycle between the ER and the Golgi apparatus and are involved in the maintenance of the Golgi structure. *Exp Cell Res* 314(19):3427–3443.
51. Anderson DJ, Hetzer MW (2008) Reshaping of the endoplasmic reticulum limits the rate for nuclear envelope formation. *J Cell Biol* 182(5):911–924.
52. Abecasis GR, Cherny SS, Cookson WO, Cardon LR (2001) GRR: Graphical representation of relationship errors. *Bioinformatics* 17(8):742–743.
53. O'Connell JR, Weeks DE (1998) PedCheck: A program for identification of genotype incompatibilities in linkage analysis. *Am J Hum Genet* 63(1):259–266.
54. Abecasis GR, Cherny SS, Cookson WO, Cardon LR (2002) Merlin—rapid analysis of dense genetic maps using sparse gene flow trees. *Nat Genet* 30(1):97–101.
55. Gudbjartsson DF, Jonasson K, Frigge ML, Kong A (2000) Allegro, a new computer program for multipoint linkage analysis. *Nat Genet* 25(1):12–13.
56. Rüschendorf F, Nürnberg P (2005) ALOHOMORA: A tool for linkage analysis using 10K SNP array data. *Bioinformatics* 21(9):2123–2125.
57. Hertel N, Redies C (2011) Absence of layer-specific cadherin expression profiles in the neocortex of the reeler mutant mouse. *Cereb Cortex* 21(5):1105–1117.
58. Viesselmann C, Ballweg J, Lumbard D, Dent EW (2011) Nucleofection and primary culture of embryonic mouse hippocampal and cortical neurons. *J Vis Exp* 47(47):2373.
59. Saengsawang W, et al. (2012) The F-BAR protein CIP4 inhibits neurite formation by producing lamellipodial protrusions. *Curr Biol* 22(6):494–501.
60. Wyatt PJ (1993) Light scattering and the absolute characterization of macromolecules. *Anal Chim Acta* 272:1–40.